A New Model of Fault-Tolerant Predictive Current Control of Multilevel Cascaded H-Bridge Inverters for Induction Motors

Mai Van Chung
Faculty of Engineering Technology, Hung Vuong University, Vietnam
maichung@hvu.edu.vn

Vo Thanh Ha
Faculty of Electrical and Electronic Engineering, University of Transport and Communications, Vietnam
vothanhha.ktd@utc.edu.vn (corresponding author)

Received: 17 April 2024 | Revised: 7 May 2024 | Accepted: 10 May 2024

 DOI: https://doi.org/10.48084/etasr.7532

ABSTRACT

This study proposes a fault-tolerant method for controlling multilevel inverters using predictive control strategies to tackle semiconductor valve open circuit problems, making a substantial step towards ensuring smooth functionality and sustained performance. The proactive error detection mechanism, based on analyzing differences between the output voltage and the H-bridge control signals, offers a sophisticated approach to fault management. With an advanced SVM voltage modulation algorithm, the system efficiently handles potential faults by optimizing switching combinations to achieve standard voltage vectors. This method ensures maximum output voltage and maintains balanced operation across three phases, resulting in an optimal operational state. The viability and effectiveness of the proposed solution are conclusively established through a comprehensive analysis and rigorous testing. MATLAB simulations confirmed the integrity of the proposed method, demonstrating its ability to accurately address current, torque, and speed requirements. The findings highlight the competence of multilevel inverters in practice, presenting them as user-friendly, secure, and capable of meeting diverse quality standards.

Keywords-MPC; IM; FOC; cascaded H-bridge; SVM

I. INTRODUCTION

This study examines a motor powered by a multi-level inverter and controlled deploying the vector method based on rotor flux and direct torque. The multilevel inverter plays a crucial role in the structure of this drive system, controlling its speed, torque, and position and ascertaining the necessary performance quality [1-3]. This is a research field that attracts the interest of scientists who explore advanced and intelligent control solutions. Multilevel inverters facilitate the use of small semiconductor devices, improving accessibility in the device thermal design process and providing an output voltage with low total harmonic distortion and dv/dt voltage variation rate [4-6]. However, the employment of multilevel inverters requires significant computational time, complexity, and extended durations for hardware and software development [7]. Furthermore, as the number of levels increases, the probability of failure in one or more semiconductor valves also increases, accounting for 38% of the errors in multilevel inverters [8-10]. In a multilevel inverter failure, the protective device disconnects it from the power grid, halting the motor [11]. Abrupt engine stopping can lead to issues such as water hammer in high-head pumping systems [12]. The prolonged operation of a faulty multilevel inverter can lead to an unbalanced output voltage, posing a risk to the motor [13]. Therefore, a fault-tolerant control solution with swift, reliable, and efficient computation time is essential.

MPC helps to address lingering issues of space vector modulation, such as optimizing the switching frequency as simultaneous cutting and suppressing of standard mode voltage is unattainable [14-15]. Moreover, to improve the reliability of the proposed solutions in multilevel inverter control, considering semiconductor valve failures is crucial. The relevance of these solutions in theoretical and practical research is evident in medium-pressure transmission systems and high-capacity motors [16-18]. In light of these advancements, integrating fault-tolerant control mechanisms becomes paramount to ensure the stability and longevity of power systems relying on multilevel inverters. By incorporating predictive control strategies, such as MPC and FCS-MPC, operators can mitigate the risks associated with inverter failures as well as optimize system performance and efficiency. The adaptability and versatility of these control methods make them well-suited for a wide range of applications, from high-head pumping systems to medium-pressure transmission setups.

Continuing research and development in this area will be instrumental in shaping the future of multilevel inverter technology and its applications in various industrial sectors [19].

This study proposes a strategy to address open circuit issues in semiconductor valves implementing a novel model predictive control algorithm to enhance the reliability of an asynchronous motor drive system powered by a cascaded H-bridge inverter [20-22]. The system proactively identifies errors by comparing the output voltage with the control signal of each H-bridge, employing an enhanced SVM voltage modulation algorithm. By analyzing the impact of faulty H-bridges, an optimal switching combination is chosen to generate the standard voltage vector, achieving objectives, like maximum output voltage, balanced three-phase operation, and optimal standard mode. Subsequently, this study evaluates the effects of errors, with and without the predictive control algorithm for error correction. The results demonstrate a significant improvement in system performance by applying the novel model predictive control algorithm, effectively reducing open circuit issues in semiconductor valves [23]. The enhanced SVM voltage modulation algorithm plays a crucial role in error detection and correction, leading to enhanced reliability and efficiency of the asynchronous motor drive systems. In general, the suggested strategy exhibits promising results in mitigating errors and optimizing the operation of a cascaded H-bridge inverter [24]. This study presents two main advancements in managing medium-voltage transmission systems for asynchronous motors using multi-level H-bridge inverters:

- Initially, an enhanced predictive controller is devised to confine the common mode voltage, optimize the switching frequency, and operate seamlessly even in semiconductor valve malfunctions within the rotary transmission system. A multilevel H-bridge inverter fuels the asynchronous direction.
- Furthermore, both the simulation and experimental results showcase the efficacy of the enhanced predictive controller in an AC drive system concerning speed, torque, and current responses. The proposed method is validated through practical models, affirming its applicability in the real world. This contribution facilitates the practical implementation of multilevel inverters, making the process straightforward, secure, and capable of meeting various quality standards.

The findings of this study can help engineers design and operate medium-voltage electric drive systems with motors powered by multilevel inverters under fault conditions. Specifically, the proposed solution can enhance the reliability of the AC transmission system. The results were validated through experimental models that illustrate practical feasibility. This study helps simplify, secure, and meet various technical needs when applying multilevel inverters, providing valuable insights for engineers working on medium-voltage electric drive systems, and offering a robust solution to improve system reliability and performance under fault conditions. In general, this study contributes to the advancement of electric drive systems and multilevel inverter technology, offering practical benefits to engineers and practitioners in the industry.

II. THE DISCRETE MODEL OF AN INDUCTION MOTOR

The asynchronous motor is controlled using Flux-Oriented Control (FOC). Based on [19], the system of equations in (1) describes the asynchronous squirrel cage rotor written on the dq coordinate system. This method allows precise control of the motor's speed and torque, making it suitable for various industrial applications. Additionally, the FOC control method offers improved efficiency and performance compared to traditional control techniques.

$$\begin{cases} \frac{di_{s\alpha}}{dt} = -\left(\frac{1}{\sigma T_s} + \frac{1-\sigma}{\sigma T_r}\right) i_{s\alpha} + \frac{1-\sigma}{\sigma T_r}\psi'_{r\alpha} + \frac{1-\sigma}{\sigma}\omega\psi'_{r\beta} + \frac{1}{\sigma L_s}u_{s\alpha} \\ \frac{di_{s\beta}}{dt} = -\left(\frac{1}{\sigma T_s} + \frac{1-\sigma}{\sigma T_r}\right) i_{s\beta} - \frac{1-\sigma}{\sigma}\omega\psi'_{r\alpha} + \frac{1-\sigma}{\sigma T_r}\psi'_{r\beta} + \frac{1}{\sigma L_s}u_{s\beta} \\ \frac{d\psi'_{r\alpha}}{dt} = \frac{1}{T_r}i_{s\alpha} - \frac{1}{T_r}\psi'_{r\alpha} - \omega\psi'_{r\beta} \\ \frac{d\psi'_{r\beta}}{dt} = \frac{1}{T_r}i_{s\beta} + \omega\psi'_{r\alpha} - \frac{1}{T_r}\psi'_{r\beta} \end{cases} \quad (1)$$

The rotor flux reciprocation angle ϑ_s, when the angular speed ω_s of the rotor flux is known, is calculated using:

$$\omega_s = \frac{d\vartheta_s}{dt} \rightarrow \vartheta_s = \vartheta_{s0} + \int_0^t \omega_s . d\tau \quad (2)$$

The motion equation is represented by:

$$M_M = M_L + \frac{J}{p_c}.\frac{d\omega}{dt} \quad (3)$$

The moment equation is expressed by:

$$M_M = \frac{3}{2}\frac{L_m^2}{L_r} z_p \psi'_{rd} i_{sq} \quad (4)$$

Considering a case when there is an error. For the system to continue working, it is necessary to detect the error, restructure the system, and perform modulation with the new structure. For transmission systems, when a semiconductor valve error occurs, the output voltage of the multilevel inverter will change (decrease). Thus, for the transmission system to continue working safely or stop actively, it is necessary to change the amount set to the engine. Based on the condition of constant overload capacity and ignoring stator resistance, the following relationship is extracted:

$$\frac{U'_S}{U_S} = \frac{f'_S}{f_S}.\sqrt{\frac{M'}{M}} = \frac{\omega'}{\omega}\sqrt{\frac{M'}{M}} \quad (5)$$

where U_S, M, and ω are the voltage, torque, and motor speed, respectivelly, when the power supply frequency is f_S. U'_S, M', and ω' are the voltage torque and motor speed when the power supply frequency is f_S. Thus, with the maximum voltage that the inverter can modulate (6), the maximum speed that the motor can achieve for the blower load is ($M_C \sim \omega^2$).

$$\omega N \sqrt{\frac{U_{Smax}}{U_{SN}}}_{max} \quad (6)$$

where U_{SN} and ω_N are the voltage amplitude on the stator phase and the motor speed when working in rated mode, and U_{Smax} is the maximum voltage amplitude on the phase that the inverter can modulate. Proceeding to discretize (1) by approximating the signal, the system of equations for the intermittent state model of the IM motor is written as:

$$\frac{di_{s\alpha}}{dt} \approx \frac{i_{s\alpha}[k+1]-i_{s\alpha}[k]}{T}, \frac{di_{s\beta}}{dt} \approx \frac{i_{s\beta}[k+1]-i_{s\beta}[k]}{T} \quad (7)$$

$$\frac{d\psi'_{r\alpha}}{dt} \approx \frac{\psi'_{r\alpha}[k+1]-\psi'_{r\alpha}[k]}{T}, \frac{d\psi'_{r\beta}}{dt} \approx \frac{\psi'_{r\beta}[k+1]-\psi'_{r\beta}[k]}{T} \quad (8)$$

The equations that predict the stator current i_s and the rotor flux ψ_r at time k+1 are written as :

$$\begin{cases} i_{s\alpha}(k+1) = \left(1-\frac{T}{\sigma T_s}-T\frac{1-\sigma}{\sigma T_r}\right)i_{s\alpha}(k) + \\ T\frac{1-\sigma}{\sigma T_r}\psi'_{r\alpha}(k) + T\frac{1-\sigma}{\sigma}\omega(k)\psi'_{r\beta}(k) + T\frac{1}{\sigma L_s}u_{s\alpha}(k) \\ i_{s\beta}(k+1) = \left(1-\frac{T}{\sigma T_s}-T\frac{1-\sigma}{\sigma T_r}\right)i_{s\beta}(k) - \\ T\frac{1-\sigma}{\sigma}\omega(k)\psi'_{r\alpha}(k) + T\frac{1-\sigma}{\sigma T_r}\psi'_{r\beta}(k) + T\frac{1}{\sigma L_s}u_{s\beta}(k) \end{cases} \quad (9)$$

The rotor flux quasi-coordinate system is written as:

$$\begin{cases} \psi'_{rd}[k] = \frac{T}{T_r}i_{sd}[k-1] + \left(1-\frac{T}{T_r}\right)\psi'_{rd}[k-1] \\ \theta_s[k] = \theta_s[k-1] + T\left(\frac{i_{sq}[k-1]}{T_r.\psi'_{rd}[k-1]} + \omega[k-1]\right) \end{cases} \quad (10)$$

III. DESIGN MODEL PREDICTIVE CURRENT CONTROLLER

Figure 1 depicts the predictive control structure with a multilevel inverter powering the asynchronous motor, combined with error detection and handling, built according to the rotor flux-like control principle. Figure 1 portrays an enhanced FCS-MPC control structure encompassing additional objectives, involving common mode voltage suppression and switching optimization. In addition, the multilevel inverter combines the strategy of detecting and handling errors when the voltage drops. At the same time, this control structure needs to adjust the flux and torque controller as required. The stator current controller ensures the smallest current deviation through the objective function.

The FCS-MPC controller for an 11-level load-connected inverter system with an asynchronous motor has the following objective function:

$$g_0 = (i_\alpha^*[k+1] - i_\alpha[k+1])^2 + \left(i_\beta^*[k+1] - i_\beta[k+1]\right)^2 \quad (11)$$

where $\left(i_\alpha^*[k+1]; i_\beta^*[k+1]\right)$ is the value of the components of the reference current, $\left(i_\alpha[k+1]; i_\beta[k+1]\right)$ is the value of the components of the predictive current $[k+1]$, and T_s is small enough, thus $i_\alpha^*[k+1] \approx i_\alpha^*[k]$ and $i_\beta^*[k+1] \approx i_\beta^*[k]$.

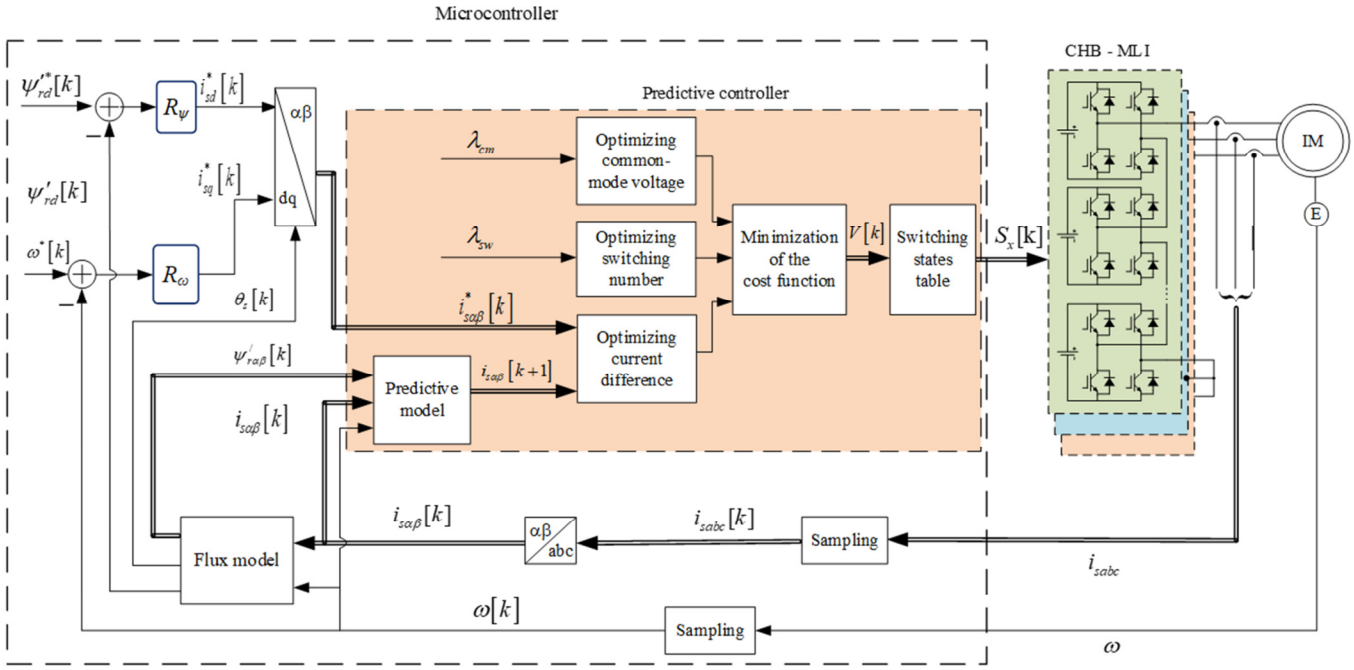

Fig. 1. The control structure of the improved FCS-MPC algorithm for the multilevel inverter system connected to the motor load.

In the objective function (11), each potential voltage vector of the system will be evaluated. The 11-level H-bridge cascading inverter comprises a total of 331 standard voltage vectors. Consequently, (1) will be assessed 331 times during each sampling cycle. The inverter's modulation will include the voltage vector that minimizes the objective function. Subsequently, the valve switching state is determined to achieve the desired output voltage vector based on the H-bridge's modulation involvement. Therefore, this meticulous evaluation ensures that the optimal voltage vector is selected to drive the inverter's modulation, leading to precise control over the switching state of the valves. The system can achieve the desired output voltage vector with high accuracy and efficiency by iteratively analyzing the potential voltage vectors and selecting the one that minimizes the objective function. This systematic approach forms the backbone of the H-bridge cascading inverter's modulation strategy, allowing for effective control and regulation of the output voltage to meet the

system's specific requirements. However, to streamline the calculation of 331 standard voltage vectors, the FCS-MPC predictive controller integrates an additional objective function that focuses on common mode voltage suppression and structural switching optimization. This added function boosts the controller's performance by efficiently handling standard mode voltages and optimizing structural switching patterns. By integrating these aspects into the control strategy, the controller can effectively reduce the computational load linked to numerous standard voltage vectors, thus enhancing overall system efficiency and performance. The proposed objective function for the enhanced MPC control method for a multilevel inverter with a cascaded H-bridge structure is:

$$g = g_0 + \lambda_{cm} g_1 + \lambda_{sw} g_2 \quad (12)$$

where λ_{cm} is the weight of common mode voltage suppression, and λ_{sw} is the weight of the switching optimization. Thus, the objective function includes three requirements:

- Optimizing the difference between the set current and the predicted current is performed by following (12).
- Common mode optimization is performed by:

$$g_1 = \frac{|v_{ZN}[k]|}{V_{dc}} \quad (13)$$

where $v_{ZN}[k]$ is the common-mode voltage at the k.

- Switching optimization is performed by g_2:

$$g_2 = |k_A[k] - k_A[k-1]| + |k_B[k] - k_B[k-1]| + |k_C[k] - k_C[k-1]| \quad (14)$$

where k_A, k_B, and k_C is the three-phase output voltage level of the inverter.

These weights are used according to the algorithm shown in Figure 2. In case a semiconductor valve error occurs, for the controller to continue working, it is necessary to detect the error, restructure the cascading H-bridge multilevel inverter circuit, and eliminate the faulty voltage vectors by relimiting or setting the amount of the input quantity. The proposed method detects the error location based on the abnormality of the output voltage on the H-bridge. The output voltage of the H-bridge is measured, normalized, and then compared with the corresponding control signal. These two signals are observed responding to that demand. When there is an abnormal deviation beyond the given conditions, the H-bridge is considered faulty and needs to be removed from the system to maintain stability. Figure 3 illustrates a block diagram of error detection.

Figure 3 presents the block diagram of the CHB-MLI open circuit fault detection method. The actual output voltage $V_{out\_cell\_i}$ of the i^{th} H-bridge is measured for normalization. The normalized output signal V_{c_cellx} is compared with the conditioning signal KH_{cellx} (voltage level on the bridge according to modulation) of that H-bridge. When monitoring two signals, if the conditions of the two counters $T1$ and $T2$ are exceeded, the fault signal is set to 1, and the H-bridge is considered faulty and is removed.

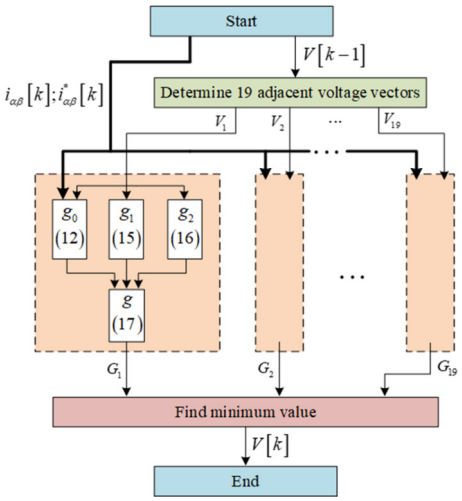

Fig. 2. Algorithm flowchart for implementing the FCS-MPC method.

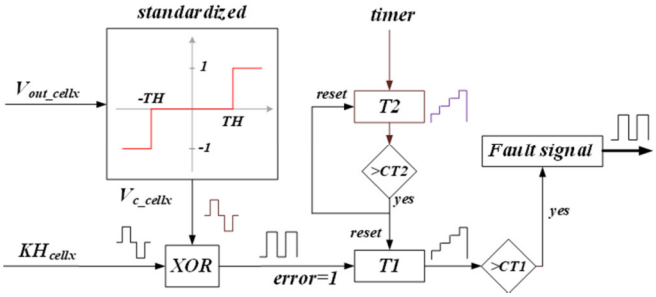

Fig. 3. Block diagram of error detection.

IV. SIMULATION RESULTS

A. Simulation Results in the Case of No Semiconductor Valve Error

The correctness and efficiency of the improved MPC algorithm were examined for a three-phase 11-level H-bridge cascade inverter supplying power to the motor connected to the blower and elevator loads. The simulation scenarios were verified by simulation in MATLAB-Simulink. The simulation was performed with sampling cycle $T = 50$ μs and inertial moment of the IM motor $J = 10$ kg.m^2.

1) Simulation with Fan Load

The simulation scenario includes the stages of motor magnetization, acceleration, and stabilization. Table I discloses the setting values for the flux and speed controllers.

TABLE I. SETTING VALUES FOR THE FLUX AND SPEED CONTROLLERS

Time (s)	0	0.7
Flux reference	7.4	
Speed reference	0	1470

With the load being a fan, the load moment is determined:

$$M_t = \left(\frac{M_{dm}}{n_{dm}^2}\right).n^2 \quad (15)$$

where M_{dm} and n_{dm} are the rated torque and rated speed of the motor, and n is its instantaneous speed. During the acceleration phase, the error value of the current is very large, so the weighting components that optimize the common-mode voltage and the number of semiconductor valve switching times are only used when the motor has reached stable speed. Table II provides the detailed values of the weights in each survey period. Figures 4, 5, and 6 display the response results of the flux, speed, and torque controllers.

TABLE II. WEIGHT VALUES IN SURVEY PERIODS

Time (s)	0 – 0.9	0.9 – 1.3	1.3 – 1.5	1.5 – 1.9
Optimal weighting of common-mode voltage	0	50	0	50
Time(s)	0 – 1.1	1.1 - 1.3	1.3 - 1.7	1.7 – 1.9
Optimal switching weight	0	6	0	6

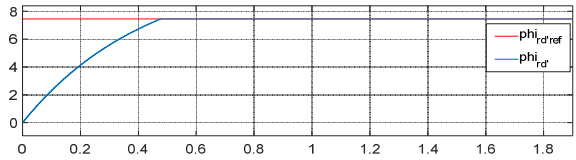

Fig. 4. Flux response.

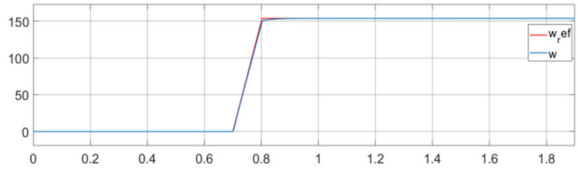

Fig. 5. Speed response.

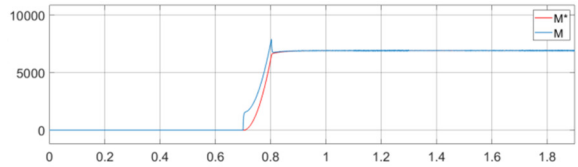

Fig. 6. Torque response.

Figure 4 demonstrates that the transient time of the motor flux is 0.47 s. Meanwhile, Figure 5 shows that when the motor rotates forward, its speed does not appear to have an overshoot, the transient time is 0.1 s, and the speed of the motor responds very well. Figure 6 indicates that the torque response of the IM motor is very good with a maximum pulse rate of 1%.

Figures 7 and 8 display the phase current and voltage responses. Figure 7 reveals that the current closely follows the set value. According to Figure 8, utilizing the optimal weighting component for common mode voltage completely eliminates it. This success signifies the effective execution of the control strategy, substantially minimizing the common mode voltage. The robust performance observed emphasizes the efficiency of the proposed approach in achieving the desired control goals.

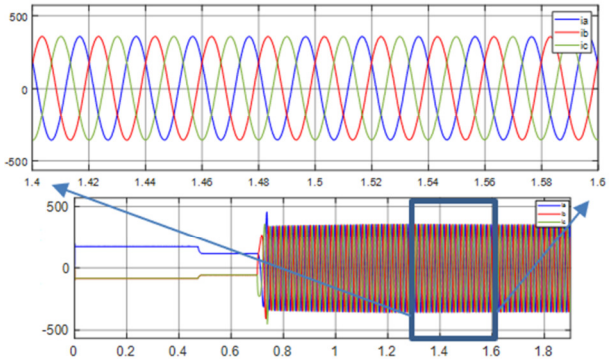

Fig. 7. Phase current response.

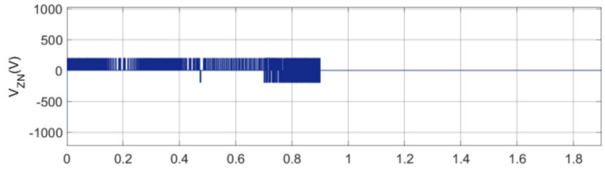

Fig. 8. Phase voltage response.

2) Simulation with Constant Load

The simulation scenario involving a constant load consists of four stages: motor magnetization, acceleration, stabilization, and rotation reversal. Table I depicts the setting values for the flux and speed controllers. During acceleration, the current error value is significant, so the weighting components optimizing the common mode voltage and semiconductor valve switching times are applied only after the motor reaches a stable speed. Table II portrays the weight values for each stage. Initially, the motor's load torque is set to 0 until 0.5 s after which it equals the motor's rated torque value.

TABLE III. SETTING VALUES FOR THE FLUX AND SPEED CONTROLLERS

Time (s)	0-0.5	0.5-1.9
Torque (Nm)	0	6906

The response results of the flux, speed, torque, and current controllers are spotted in Figures 9-12.

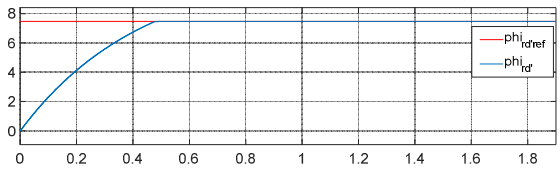

Fig. 9. Flux response.

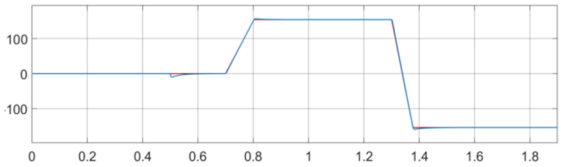

Fig. 10. Speed response.

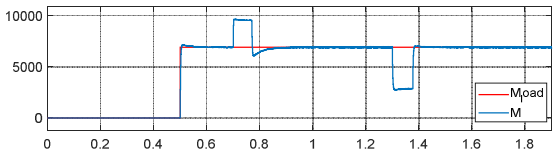

Fig. 11. Torque response.

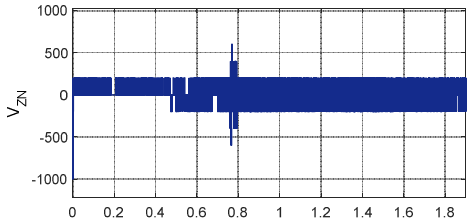

Fig. 12. Voltage response.

The simulation results in Figure 9 showcase that the transient time of the motor flux is 0.47 s. Meanwhile, in the simulation results of Figure 10, when the motor rotates forward, the motor speed has an overcorrection of 2.1% and the transient time is 0.17 s. When the motor rotates in reverse, the motor speed appears overcorrected by 3% and the transient time is 0.05 s. Therefore, it is noticed that the speed of the motor responds very quickly. The simulation results displayed in Figure 11 demonstrate that the motor torque has a very favorable response, reaching a maximum pulse rate of 1%. Figure 12 indicates that when utilizing the optimal weighting component for the common-mode voltage, a complete voltage suppression occurs. This phenomenon is crucial to ensure the integrity and efficiency of the system, particularly in scenarios where common-mode interference can significantly affect performance. By effectively utilizing the optimal weighting component, as observed in Figure 12, the system exhibits a remarkable ability to mitigate common mode voltage disturbances, thus enhancing overall operational stability and reliability.

B. Simulation Results with Semiconductor Valve Failure Case

The IM motor transmission simulation scenario is governed by the MPC control algorithm, as shown in Table IV.

TABLE IV. THE SETTING VALUES FOR THE FLUX AND SPEED CONTROLLERS

Time (s)	0 - 0.4 s	0.4 - 1 s	1 - 1.5 s	1.5 - 2 s	2 - 2.5 s
Speed (rmp)	0	0→1470	1470	1470	1470
Errors of H-bridges	0	0	0	H_{A1}	H_{A1}, H_{A3}, H_{B1}

1) Evaluation of Transmission System Speed

Figure 13 illustrates the IM motor speed response in case of semiconductor valve error. There is no CHB-MLI error in the range of 0 to 1.5 s. The engine speed sticks to the set value and operates stably at the rated speed of 1470 rpm, and the FOC algorithm operates normally. In the range of 1.5 to 2s, when a problem occurs at HA_1, as the error voltage vector is eliminated and the voltage value that can be generated by CHB-MLI is greater than the motor's rated voltage, the system works normally. Between 2 and 2.5 s, bridges HA_1, HA_3, and HB_1 had errors at the same time, but the speed was stable because the voltage was limited, thereby limiting the speed.

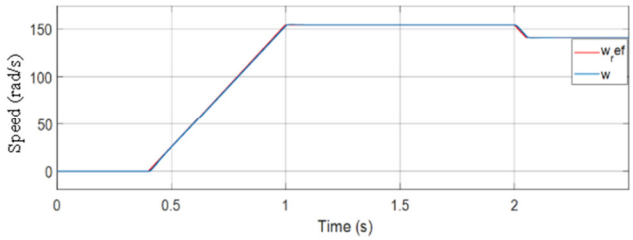

Fig. 13. Speed response with current predictive control method under power valve fault conditions.

2) Evaluation of Torque

Figure 14 presents the motor torque generated in the three scenarios. Figure 14 shows the torque response results from the current prediction control method, indicating that the torque response of this method is quicker when the speed response following the quality limit is enhanced.

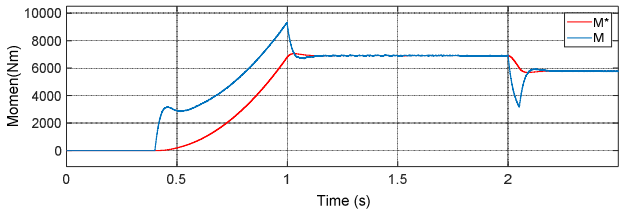

Fig. 14. Torque response with current predictive control method under power valve fault conditions.

Based on the findings provided in Figure 14:

- Between 0 and 1.5 s, the torque remains steady at 7380Nm in the absence of errors.
- From 1.5 to 2 s, with an error in the HA_1 bridge, the controller eliminates the error voltage vector, causing the inverter's output voltage to exceed the motor's rated voltage, therefore maintaining stable torque.
- Between 2 and 2.5 s, bridges HA_1, HA_3, and HB_1 experience simultaneous errors. The controller restricted the torque due to speed limitations imposed by the voltage cap. Despite the decrease in torque, the pulse rate remained nearly constant. The torque response analysis from the current prediction control method indicates that this method's torque response is quicker when the speed response improves after reaching the quality limit.

C. Evaluation of the Output Voltage

As observed in Figure 15, the line voltage response ensures balance when an error occurs. The simulation results disclose that:

- During about 2 to 2.5 s, when there is a simultaneous HA_1, HA_3, and HB_1 error, the status level of phase A is only [-3, 3] because the HA_1 bridge on phase A has been removed.

Phase B is only [-4, 4] due to the removal of bridge HB_1, and phase C is not defective in this error.

- From 1.5 to 2s, the HA_1 bridge has an error but the output voltage exceeds the inverter's rated voltage, maintaining the voltage.
- Around 2 to 2.5s, with simultaneous errors in HA_1, HA_3, and HB_1, the inverter's voltage output falls below the motor's rated voltage, leading to a limitation and equivalent reduction in voltage. Operating speed drops below standard levels.

Figure 16 depicts the phase voltage pattern.

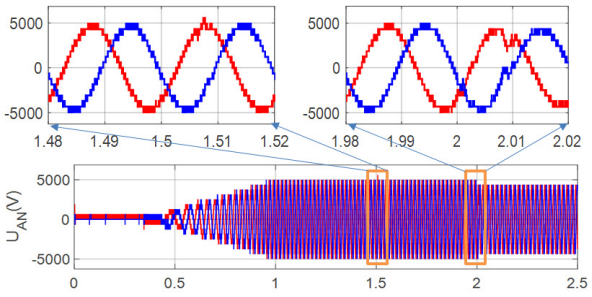

Fig. 15. Shape of line voltage with current predictive control method under power valve fault condition.

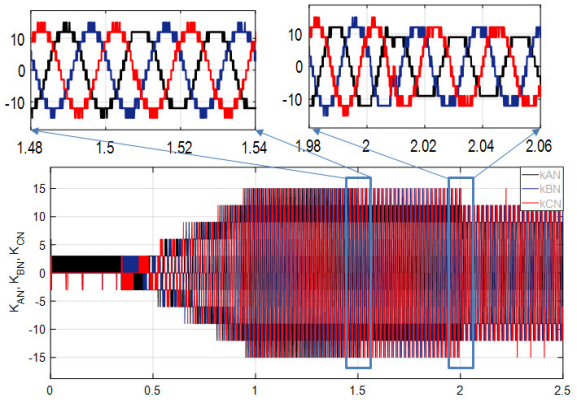

Fig. 16. The shape of phase voltage with current predictive control method.

The simulation results in Figure 16 manifest that:

- Between 1.5s and 2s, an error in the HA_1 bridge limits phase A to [-4, 4] as the HA_1 bridge is disconnected. Phases B and C remain at zero change to [-5, 5].
- At approximately 2 to 2.5s, HA_1, HA_3, and HB_1 errors lead to phase A being restricted to [-3, 3] due to HA_1's removal. Phase B is limited to [-4, 4] because of HB1's removal. Phase C is unaffected by the error and is also constrained to [-4, 4].

The CHB-MLI prediction controller considers the problem when powering the asynchronous drive system and obtains the following results: voltage and current are limited to ensure the smallest drop is equally balanced. Speed is limited through voltage limitation. From there, the transmission system can maintain operation or actively stop the system. The results acquired are equivalent to the case applied in the FOC-IM control method because they are limited by the space vector modulation method for CHB-MLI error conditions. During about 2 to 2.5 s, when there is a simultaneous HA_1, HA_3, and HB_1 error, the status level of phase A is only [-3, 3] because the HA_1 bridge on phase A has been removed. Phase B is only [-4, 4] due to the removal of bridge HB_1 and phase C is not defective due to the influence of the error and is also limited to only [-4, 4].

V. CONCLUSIONS

This study successfully developed an improved MPC controller with integrated error detection and handling algorithms for an asynchronous motor drive system powered by an 11-level H-bridge inverter to enhance reliability and sustainability during operation. Simulation results demonstrated the effectiveness of the upgraded predictive controller in terms of speed, torque, and current responses. This advancement streamlines operations, enhances security, and meets various quality standards for multilevel inverters. Moreover, it assists engineers in designing and managing electric drive systems with multilevel inverter-powered motors, even under fault conditions. Simulation models confirmed the research results, highlighting practical applicability. Additionally, the seamless integration of the 11-level H-bridge inverter optimizes energy efficiency and reduces harmonic distortions, aligning with contemporary sustainability objectives. However, for enhanced reliability, deployment of this controller to real devices and comparative evaluation against other common control methods are necessary.

ACKNOWLEDGMENT

This research was funded by Hung Vuong University under grant number HV22.2023.

REFERENCES

[1] B. Wu and M. Narimani, "Cascaded H-Bridge Multilevel Inverters," in *High-Power Converters and AC Drives*, Wiley-IEEE Press, 2017, pp. 119–141.

[2] J. S. Lai and F. Z. Peng, "Multilevel converters-a new breed of power converters," *IEEE Transactions on Industry Applications*, vol. 32, no. 3, pp. 509–517, Feb. 1996, https://doi.org/10.1109/28.502161.

[3] M. Marchesoni, M. Mazzucchelli, and S. Tenconi, "A nonconventional power converter for plasma stabilization," *IEEE Transactions on Power Electronics*, vol. 5, no. 2, pp. 212–219, Apr. 1990, https://doi.org/10.1109/63.53158.

[4] B. H. Kumar, M. M. Lokhande, R. R. Karasani, and V. B. Borghate, "Fault Tolerant Operation of CHB Multilevel Inverters Based on the SVM Technique Using an Auxiliary Unit," *Journal of Power Electronics*, vol. 18, no. 1, pp. 56–69, 2018, https://doi.org/10.6113/JPE.2018.18.1.56.

[5] D. G. Holmes and T. A. Lipo, Pulse Width Modulation for Power Converters: Principles and Practice. John Wiley & Sons, 2003.

[6] B. Lu and S. K. Sharma, "A Literature Review of IGBT Fault Diagnostic and Protection Methods for Power Inverters," *IEEE Transactions on Industry Applications*, vol. 45, no. 5, pp. 1770–1777, Sep. 2009, https://doi.org/10.1109/TIA.2009.2027535.

[7] Y. Zhang, B. Xia, and H. Yang, "Performance evaluation of an improved model predictive control with field oriented control as a benchmark," *IET Electric Power Applications*, vol. 11, no. 5, pp. 677–687, 2017, https://doi.org/10.1049/iet-epa.2015.0614.

[8] M. P. Kazmierkowski and L. Malesani, "Current control techniques for three-phase voltage-source PWM converters: a survey," *IEEE Transactions on Industrial Electronics*, vol. 45, no. 5, pp. 691–703, Jul. 1998, https://doi.org/10.1109/41.720325.

[9] S. Kouro, P. Cortes, R. Vargas, U. Ammann, and J. Rodriguez, "Model Predictive Control—A Simple and Powerful Method to Control Power Converters," *IEEE Transactions on Industrial Electronics*, vol. 56, no. 6, pp. 1826–1838, Jun. 2009, https://doi.org/10.1109/TIE.2008.2008349.

[10] J. H. Lee, "Model predictive control: Review of the three decades of development," *International Journal of Control, Automation and Systems*, vol. 9, no. 3, pp. 415–424, Jun. 2011, https://doi.org/10.1007/s12555-011-0300-6.

[11] J. Rodriguez *et al.*, "Multilevel Converters: An Enabling Technology for High-Power Applications," *Proceedings of the IEEE*, vol. 97, no. 11, pp. 1786–1817, Aug. 2009, https://doi.org/10.1109/JPROC.2009.2030235.

[12] A. Nabae, I. Takahashi, and H. Akagi, "A New Neutral-Point-Clamped PWM Inverter," *IEEE Transactions on Industry Applications*, vol. IA-17, no. 5, pp. 518–523, Sep. 1981, https://doi.org/10.1109/TIA.1981.4503992.

[13] T. A. Meynard and H. Foch, "Multi-Level Choppers for High Voltage Applications," *EPE Journal*, vol. 2, no. 1, pp. 45–50, Jan. 1992, https://doi.org/10.1080/09398368.1992.11463285.

[14] T. A. Meynard, H. Foch, P. Thomas, J. Courault, R. Jakob, and M. Nahrstaedt, "Multicell converters: basic concepts and industry applications," *IEEE Transactions on Industrial Electronics*, vol. 49, no. 5, pp. 955–964, Jul. 2002, https://doi.org/10.1109/TIE.2002.803174.

[15] S. Kouro *et al.*, "Recent Advances and Industrial Applications of Multilevel Converters," *IEEE Transactions on Industrial Electronics*, vol. 57, no. 8, pp. 2553–2580, Dec. 2010, https://doi.org/10.1109/TIE.2010.2049719.

[16] S. Allebrod, R. Hamerski, and R. Marquardt, "New transformerless, scalable Modular Multilevel Converters for HVDC-transmission," in *2008 IEEE Power Electronics Specialists Conference*, Rhodes, Greece, Jun. 2008, pp. 174–179, https://doi.org/10.1109/PESC.2008.4591920.

[17] M. A. Perez, S. Bernet, J. Rodriguez, S. Kouro, and R. Lizana, "Circuit Topologies, Modeling, Control Schemes, and Applications of Modular Multilevel Converters," *IEEE Transactions on Power Electronics*, vol. 30, no. 1, pp. 4–17, Jan. 2015, https://doi.org/10.1109/TPEL.2014.2310127.

[18] A. Akpunar and S. Iplikci, "Runge-Kutta Model Predictive Speed Control for Permanent Magnet Synchronous Motors," *Energies*, vol. 13, no. 5, Jan. 2020, Art. no. 1216, https://doi.org/10.3390/en13051216.

[19] H. Bassi and Y. A. Mobarak, "State-Space Modeling and Performance Analysis of Variable-Speed Wind Turbine Based on a Model Predictive Control Approach," *Engineering, Technology & Applied Science Research*, vol. 7, no. 2, pp. 1436–1443, Apr. 2017, https://doi.org/10.48084/etasr.1015.

[20] D. T. Tu, "Enhancing Road Holding and Vehicle Comfort for an Active Suspension System utilizing Model Predictive Control and Deep Learning," *Engineering, Technology & Applied Science Research*, vol. 14, no. 1, pp. 12931–12936, Feb. 2024, https://doi.org/10.48084/etasr.6582.

[21] P. Weyers, A. Barth, and A. Kummert, "Driver State Monitoring with Hierarchical Classification," in *2018 21st International Conference on Intelligent Transportation Systems (ITSC)*, Maui, HI, USA, Nov. 2018, pp. 3239–3244, https://doi.org/10.1109/ITSC.2018.8569467.

[22] V. Q. Vinh and V. T. Ha, "Improved Torque Ripple of Switched Reluctance Motors using Sliding Mode Control for Electric Vehicles," *Engineering, Technology & Applied Science Research*, vol. 13, no. 1, pp. 10140–10144, Feb. 2023, https://doi.org/10.48084/etasr.5559.

[23] C. F. Garcia, C. A. Silva, J. R. Rodriguez, P. Zanchetta, and S. A. Odhano, "Modulated Model-Predictive Control With Optimized Overmodulation," *IEEE Journal of Emerging and Selected Topics in Power Electronics*, vol. 7, no. 1, pp. 404–413, Mar. 2019, https://doi.org/10.1109/JESTPE.2018.2828198.

[24] I. Kim, R. Chan, and S. Kwak, "Model predictive control method for CHB multi-level inverter with reduced calculation complexity and fast dynamics," *IET Electric Power Applications*, vol. 11, no. 5, pp. 784–792, 2017, https://doi.org/10.1049/iet-epa.2016.0330.